https://doi.org/10.5194/tc-2020-296
Preprint. Discussion started: 11 November 2020

The Cryosphere Discussions
Open Access
EGU

21st century fate of the Mocho-Choshuenco ice cap in southern Chile

Matthias Scheiter[1,2], Marius Schaefer[3], Eduardo Flández[4], Deniz Bozkurt[5,6], and Ralf Greve[7,8]

[1]Research School of Earth Sciences, Australian National University, Canberra, Australia
[2]previously at Institut für Geophysik und Geoinformatik, TU Bergakademie Freiberg, Freiberg, Germany
[3]Instituto de Ciencias Físicas y Matemáticas, Universidad Austral de Chile, Valdivia, Chile
[4]Departamento de Física, Facultad de Ciencias, Universidad de Chile, Santiago, Chile
[5]Departamento de Meteorología, Universidad de Valparaíso, Valparaíso, Chile
[6]Center for Climate and Resilience Research (CR)2, Santiago, Chile
[7]Institute of Low Temperature Science, Hokkaido University, Sapporo, Japan
[8]Arctic Research Center, Hokkaido University, Sapporo, Japan

Correspondence: Matthias Scheiter (matthias.scheiter@anu.edu.au)

Abstract. Glaciers and ice caps are thinning and retreating along the entire Andes ridge, and drivers of this mass loss vary between the different climate zones. The southern part of the Andes (Wet Andes) has the highest abundance of glaciers in number and size, and a proper understanding of ice dynamics is important to assess their evolution. In this contribution, we apply the ice sheet model SICOPOLIS to the Mocho-Choshuenco ice cap in the Chilean Lake District (40°S, 72°W, Wet Andes) to reproduce its current state and to project its evolution until the end of the 21st century under different global warming scenarios. First, we create a model spin-up using surface mass balance data observed on the south-eastern catchment, extrapolating them to the whole ice cap using an exposition-dependent parameterization. This spin-up is able to reproduce the most important present-day glacier features. Based on the spin-up, we then run the model 80 years into the future, forced by projected surface temperature anomalies from different global circulation models under different radiative pathway scenarios to obtain estimates of the ice cap's state by the end of the 21st century. The mean projected ice volume losses are $25 \pm 19\%$ (RCP2.6), $64 \pm 14\%$ (RCP4.5) and $94 \pm 3\%$ (RCP8.5) with respect to the ice volume estimated by radio-echo sounding data from 2013. We estimate the uncertainty of our projections based on the spread of the results when forcing with different global climate models and on the uncertainty associated with the variation of the equilibrium line altitude with temperature change. Considering our results, we project an considerable deglaciation of the Chilean Lake District by the end of the 21st century.

1 Introduction

Most glaciers and ice caps in the Andes are currently thinning and retreating (e.g. Braun et al., 2019), and rates of mass loss are increasing in many places (Dussaillant et al., 2019). In the Southern part of the Andes (Wet Andes or Patagonian Andes, 36-56°S) the highest number of glaciers are found and large icefields as the Northern Patagonia Icefield, Southern Patagonia

https://doi.org/10.5194/tc-2020-296
Preprint. Discussion started: 11 November 2020

Icefield and Cordillera Darwin are located in this region. The specific mass losses observed or inferred for the glaciers of the Wet Andes are the highest in the Andes (Dussaillant et al., 2019; Braun et al., 2019) and among the highest of all glacier regions worldwide (Zemp et al., 2019).

The maritime climate of the Wet Andes is characterized by high precipitation rates of up to $10000\,\mathrm{mm\,yr^{-1}}$ on the windward side and rather mild temperatures with freezing levels generally above 1 km above mean sea level (Garreaud et al., 2013). This leads to an exceptionally high mass turnover (Schaefer et al., 2013, 2015, 2017) and high flow speeds for the glaciers in the region (Sakakibara and Sugiyama, 2014; Mouginot and Rignot, 2015). Apart from climate forcings, ice dynamics and frontal ablation are important contributors to glacier changes in the region. As these are best represented in ice-flow models, they are appropriate tools to project future behavior of the glaciers of the Wet Andes.

Only few studies have tried to project future behavior of Andean glaciers. Réveillet et al. (2015) modelled Zongo Glacier (16°S) in the tropical Andes using the 3-D full-Stokes model Elmer/Ice (developed by Gagliardini et al., 2013). They projected volume losses between 40% and 89% until the end of this century under the RCP2.6 and RCP8.5 scenarios, respectively. In the Wet Andes, Möller and Schneider (2010) projected an area loss of 35% of Glaciar Noroeste, an outlet glacier of the Gran Campo Nevado ice cap (53°S), until the end of the 21st century using a degree-day model and volume-area scaling relationships. Schaefer et al. (2013) modeled the surface mass balance (SMB) of the Northern Patagonian Icefield in the 21st century under the A1B scenario (of IPCC Assessment Report 4, comparable to RCP6.0). They projected a strongly decreasing SMB until the end of the 21st century, mainly due to an increase in surface temperature by the middle of the century and a decrease of accumulation towards the end of the century. Collao-Barrios et al. (2018) infer important committed mass loss of San Rafael Glacier under current climate applying the Elmer/Ice flow model with fixed glacier outlines.

In this contribution, our first objective is to reproduce the present-day behaviour of the Mocho-Choshuenco ice cap in the northern part of the Wet Andes (40°S) using the ice-sheet model SICOPOLIS (Greve, 1997a, b). To this end, we make use of a newly developed SMB parameterization scheme and glaciological data obtained on the ice cap to calibrate the model and reproduce its current state. Our second objective is to project the behaviour of the Mocho-Choshuenco ice cap through the course of the 21st century to provide one of the first constraints on future glacier dynamics in the Wet Andes. For this aim, we make use of temperature projections from 23 Global Climate Models (GCMs) participating in the Coupled Model Intercomparison Project phase 5 (CMIP5) (Taylor et al., 2012) under low (RCP2.6), medium (RCP4.5) and high emission (RCP8.5) scenarios as input to SICOPOLIS.

We begin this paper by describing the observational data and methods (Section 2). In Section 3, we present the results: first, we validate the model spin-up using observed glacier outlines, ice thickness and flow speed. We then present the evolution of ice cap extension and volume during the 21st century as obtained through different emission scenarios. Then, in Section 4, we discuss our results, compare them to previous studies and analyse the limitations of our approach. We conclude the paper by summarizing the main findings in Section 5.

https://doi.org/10.5194/tc-2020-296
Preprint. Discussion started: 11 November 2020

2 Methods

2.1 Observational data

In this study, we simulate the present and future state of the ice cap covering the Mocho-Choshuenco volcanic complex, which we refer to as Mocho-Choshuenco ice cap. It is located in the Chilean Lake District at 40°S, 72°W (see inset map in Figure 1). Over the last 20 years, climatological and glaciological observations have been made on the ice cap (Rivera et al., 2005; Schaefer et al., 2017). SMB data were obtained through the traditional glaciological method on a stake network on the south-eastern part of the ice cap (red stars in Figure 1). These measurements yielded an average negative SMB of $-0.9\,\mathrm{m\,w.e.\,yr^{-1}}$ (meter water equivalent per year) with an exceptionally high mass turnover of around $5\,\mathrm{m\,w.e.\,yr^{-1}}$ (Schaefer et al., 2017). This high mass turnover can be explained by climatological data: between 2006 and 2015, the annual mean temperature was $2.6°\mathrm{C}$ at an automatic weather station (green circle in Figure 1) at an elevation of $2000\,\mathrm{m}$, and therefore close to the typical equilibrium line altitude (ELA) (Schaefer et al., 2017). Mean annual precipitation over the same period was around $4000\,\mathrm{mm\,yr^{-1}}$ in Puerto Fuy at an elevation of $600\,\mathrm{m}$ to the north of the volcano.

https://doi.org/10.5194/tc-2020-296
Preprint. Discussion started: 11 November 2020

The Cryosphere
Discussions
Open Access
EGU

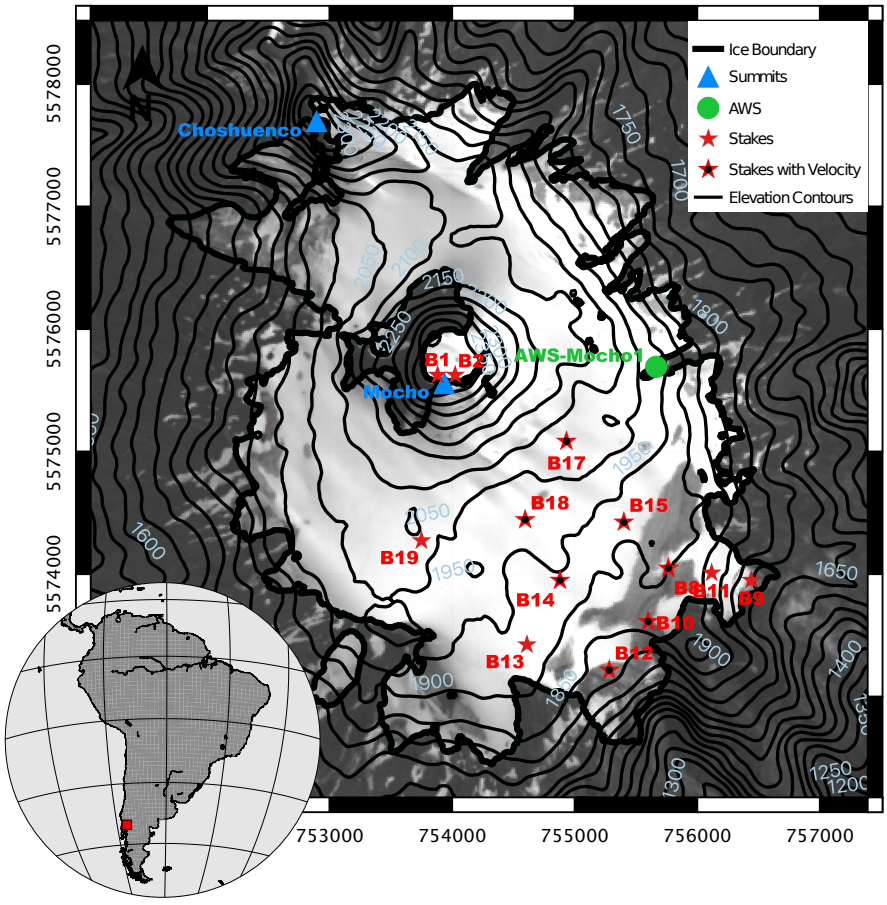

Figure 1. Overview map of the Mocho-Choshuenco ice cap with significant geographic features and measurement sites. The contour line spacing is 50 m. East and North are in UTM S18. Background: Landsat image (February 22, 2015). Inset map shows location in South America.

At some of the mass balance stakes (red stars with inner black dots in Figure 1), GPS measurements were made to infer surface flow velocity, giving typical values of around $30\,\mathrm{m\,yr^{-1}}$ (Geoestudios, 2013). Further measurements include ground penetrating radar (GPR) transects (green lines in Figure 2a) over most parts of the ice cap (Geoestudios, 2014). Through inverse distance weighting interpolation over the whole ice cap, a total ice volume of $1.038\,\mathrm{km^3}$ was obtained (Geoestudios, 2014). The interpolated ice thickness map was subtracted from a digital elevation model (TanDEM WorldDEM, acquired between 2012 and 2014) to yield a bedrock topography (Flández, 2017). We use this topography as the base of the ice cap in the simulations we perform with SICOPOLIS.

https://doi.org/10.5194/tc-2020-296
Preprint. Discussion started: 11 November 2020

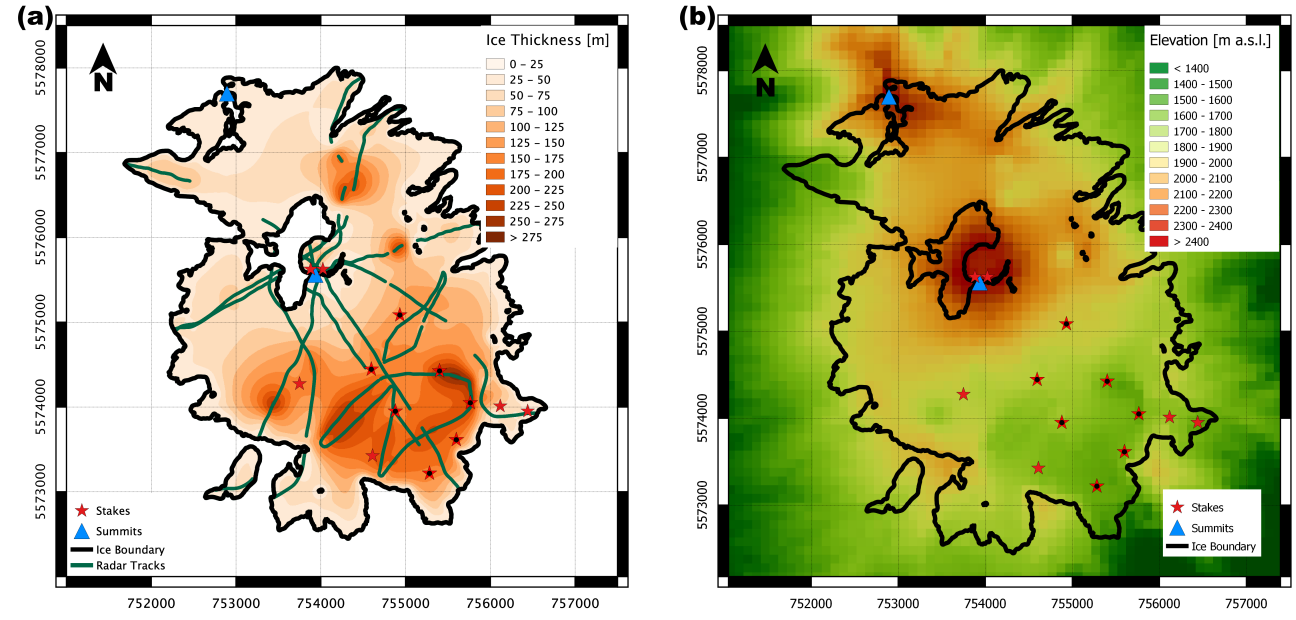

Figure 2. (a) Ground penetrating radar (GPR) transects shown in green lines together with the interpolated ice thickness. (b) Bedrock topography obtained after subtracting the interpolated ice thickness from surface elevation. This topography is used as the ice cap base in our simulations.

2.2 SICOPOLIS

The three-dimensional, dynamic/thermodynamic model SICOPOLIS (SImulation COde for POLythermal Ice Sheets) was originally created in a version for the Greenland ice sheet (Greve, 1997a, b). Since then, the model has been developed continuously and applied to problems of past, present and future glaciation of Greenland, Antarctica, the entire northern hemisphere, the polar ice caps of the planet Mars and others, resulting in more than 120 publications in the peer-reviewed literature (www.sicopolis.net). The model supports the shallow-ice approximation (SIA) for slow-flowing grounded ice, hybrid shallow-ice–shelfy stream dynamics for fast-flowing grounded ice and the shallow-shelf approximation for floating ice (Bernales et al., 2017), as well as several thermodynamics solvers (Blatter and Greve, 2015; Greve and Blatter, 2016).

Mainly developed for ice sheets, the smallest ice body to which SICOPOLIS has been applied so far is the Austfonna Ice Cap, for which Dunse et al. (2011) reproduced the observed cyclic surge behaviour under constant, present-day climate conditions. For this study, we adapted SICOPOLIS v5.1 (Greve and SICOPOLIS Developer Team, 2019) for the Mocho-Choshuenco ice cap in SIA mode. We employ a standard Glen flow law with a stress exponent of $n = 3$. Basal sliding is modelled by a linear sliding law,

$$v_\mathrm{b} = -C_\mathrm{b}\tau_\mathrm{b}\,, \tag{1}$$

https://doi.org/10.5194/tc-2020-296
Preprint. Discussion started: 11 November 2020

where v_b is the basal sliding velocity, τ_b the basal drag and C_b the sliding coefficient. The value of the latter is determined by the calibration procedure of the present-day spin-up (see Section 3.1). Since Mocho-Choshuenco is a temperate ice cap, we replaced solving the energy balance equation by keeping the temperature at a constant value of $0°\mathrm{C}$ (precisely speaking, and for technical reasons only as SICOPOLIS does not allow an all-temperate ice body, $-0.001°\mathrm{C}$). The rate factor is set to the value recommended by Cuffey and Paterson (2010) for $0°\mathrm{C}$, which is $A = 2.4 \times 10^{-24}\,\mathrm{s}^{-1}\,\mathrm{Pa}^{-3}$. To ensure proper mass conservation despite the steep slopes and rugged bed topography, we use an explicit solver for the ice thickness equation that discretizes the advection term by a mass-conserving scheme in an upwind flux form (Calov et al., 2018).

2.3 Aspect-dependent SMB parameterization

SICOPOLIS incorporates a linear altitude-dependent SMB parameterization which is visualised in Figure 3a and can be described by the following formula:

$$\mathrm{SMB}(C) = \min(S_0, M_0 \cdot (z(C) - \mathrm{ELA})). \tag{2}$$

Here, ELA is the equilibrium line altitude, $z(C)$ is the altitude of a specific grid cell C, M_0 denotes the mass balance gradient and S_0 is maximum snowfall.

From the simulations performed by Flández (2017) on the Mocho-Choshuenco ice cap it becomes apparent that the simple altitude-dependent SMB parameterization in Equation 2 is not detailed enough to account for small-scale SMB variations on the ice cap. In particular, SMB should be lower in the north-western part than in the south-eastern part of the ice cap. We therefore employ a new parameterization which is illustrated in Figure 3b. With the Mocho summit in the center, ELA should have a maximum $B_\mathrm{ELA} + A_\mathrm{ELA}$ in the direction φ_0, a minimum $B_\mathrm{ELA} - A_\mathrm{ELA}$ in the opposite direction and a mean value B_ELA on the two perpendicular directions.

https://doi.org/10.5194/tc-2020-296
Preprint. Discussion started: 11 November 2020

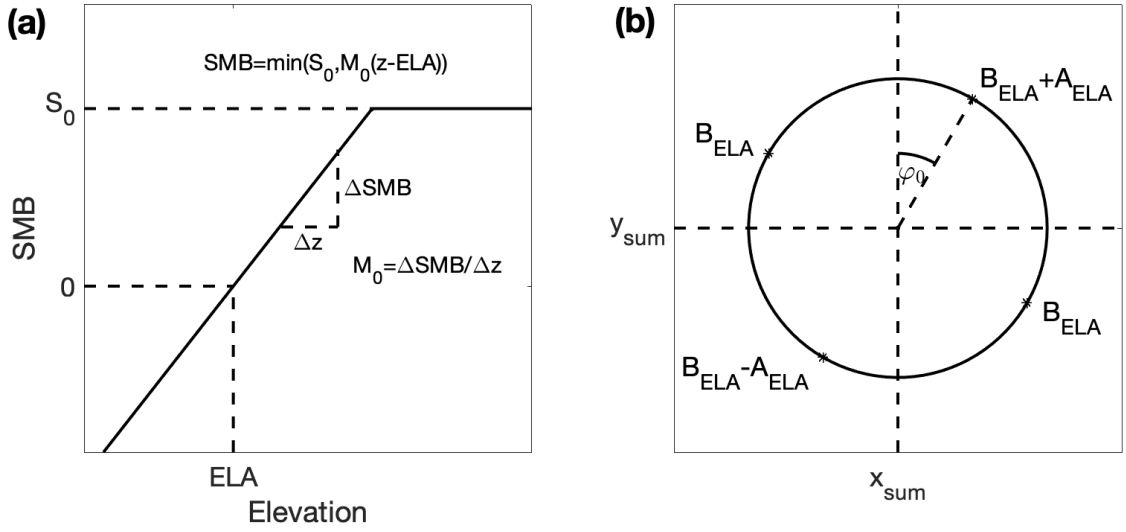

Figure 3. (a) Elevation-dependent SMB parameterization. SMB increases linearly with elevation until an upper bound S_0 and stays constant at higher elevations. (b) Aspect-dependent SMB parameterization. ELA takes a minimum and maximum on two opposite directions ($B_{\text{ELA}} \pm A_{\text{ELA}}$), and their mean ($B_{\text{ELA}}$) on perpendicular directions. φ_0 is a direction offset to rotate the values according to the atmospheric conditions. $(x_{\text{sum}}, y_{\text{sum}})$ indicates the position of Mocho summit. In this visualisation, φ_0 is set to 30°.

These values can be summarized in a cosine function in φ with the direction of maximum ELA φ_0, the amplitude A_{ELA} and an offset of the average ELA B_{ELA}:

$$\text{ELA} = A_{\text{ELA}} \cos(\varphi - \varphi_0) + B_{\text{ELA}}. \tag{3}$$

B_{ELA} is used to shift the ELA to the desired mean altitude. φ is the cardinal direction of a point with respect to the summit and can be calculated by

$$\varphi = \text{arctan2}(x - x_{\text{sum}}, y - y_{\text{sum}}), \tag{4}$$

where arctan2 denotes the two-argument arctangent and x and y are the distances in the two directions from a grid point to the summit location $(x_{\text{sum}}, y_{\text{sum}})$.

2.4 Temperature projections

The main goal of this study is to project the future evolution of the Mocho-Choshuenco ice cap. We use future temperature simulations from 23 climate models participating in CMIP5 (see Appendix A). To ease the calculations, all the models were interpolated onto a common grid of $1.5^\circ \times 1.5^\circ$ using bilinear interpolation. Then the time series of each model were extracted

https://doi.org/10.5194/tc-2020-296
Preprint. Discussion started: 11 November 2020

from the grid point corresponding to Mocho-Choshuenco ice cap (40°S, 72°W). As the model trajectories start in 2006 and in order to be consistent with the reference ice cap conditions based on the observational dataset obtained between 2009 and 2013, we used the period from 2006 to 2020 as the reference period rather than the commonly used historical periods (e.g., 1976-2005) in order to construct projections of temperature anomalies. The mean of this period (2006-2020) was then subtracted from each time series of 23 models in order to construct temperature projections. At the final step, the SICOPOLIS model was driven by each of the 23 model projection to provide a more robust assessment of future evolution of the Mocho-Choshuenco ice cap. This allows us to assess the uncertainty associated with climate model differences.

Our approach makes use of three emission scenarios following the IPCC protocols (IPCC, 2013): high-mitigation, Paris Agreement compatible (RCP2.6); medium stabilisation scenario with a peak around 2040, then decline (RCP4.5); and high-end baseline scenario with no control policies of greenhouse gas emissions (RCP8.5). This allows us to contrast the future evolution of the Mocho-Choshuenco ice cap under different emission scenarios together with the uncertainty introduced by future emissions. Figure 4 shows the projected changes in temperature obtained from 23 individual climate models for the ice cap under the three different emission scenarios until the end of the century. This yields 69 projections which are all used to run SICOPOLIS and averaged afterwards. All projections follow a similar trend until the 2040s, where the RCP8.5 scenario separates from the others and continues to increase throughout the century, leading to a model mean temperature increase of $3.15 \pm 0.69°\mathrm{C}$ by the end of the century. The temperature projections under the RCP2.6 and RCP4.5 scenarios have largely similar evolutions after the 2050s with weaker projected changes than those in RCP8.5. By the end of the century, projected temperature increases for the RCP 2.6 and RCP4.5 scenarios are $0.33 \pm 0.47°\mathrm{C}$ and $1.01 \pm 0.43°\mathrm{C}$, respectively.

https://doi.org/10.5194/tc-2020-296
Preprint. Discussion started: 11 November 2020

The Cryosphere Discussions
Open Access
EGU

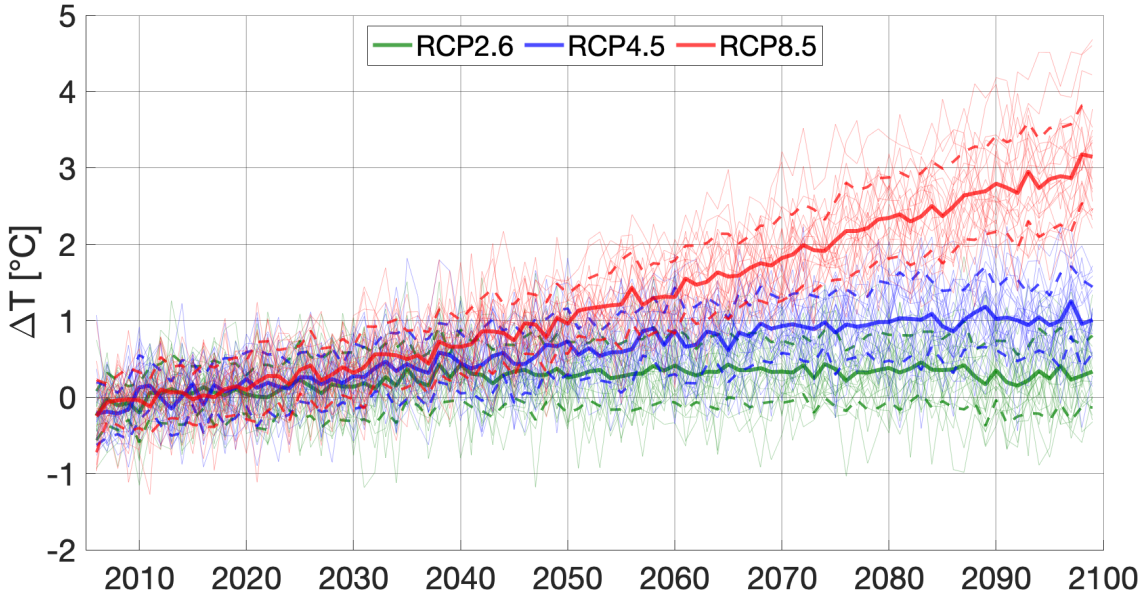

Figure 4. Temperature projections for the Mocho-Choshuenco ice cap through the 21st century for three different scenarios RCP2.6, RCP4.5 and RCP8.5. The thin lines show projections of the 23 individual climate models, thick solid lines indicate their mean and thick dashed lines the one-sigma confidence interval. The period between 2006 and 2020 is used as reference period for each individual model.

2.5 Glacier sensitivity to temperature change

135 To link the projected 21st century temperature rise to ice dynamics, it is necessary to relate the temperature anomalies to changes in SMB which is determined by the ELA in our case. For the Mocho-Choshuenco ice cap, there are four years (2009-2013) of availability of both the ELA and annual mean temperature at a similar altitude (Schaefer et al., 2017). These data are shown in Figure 5 together with the ELA error estimates.

https://doi.org/10.5194/tc-2020-296
Preprint. Discussion started: 11 November 2020

The Cryosphere Discussions
Open Access
EGU

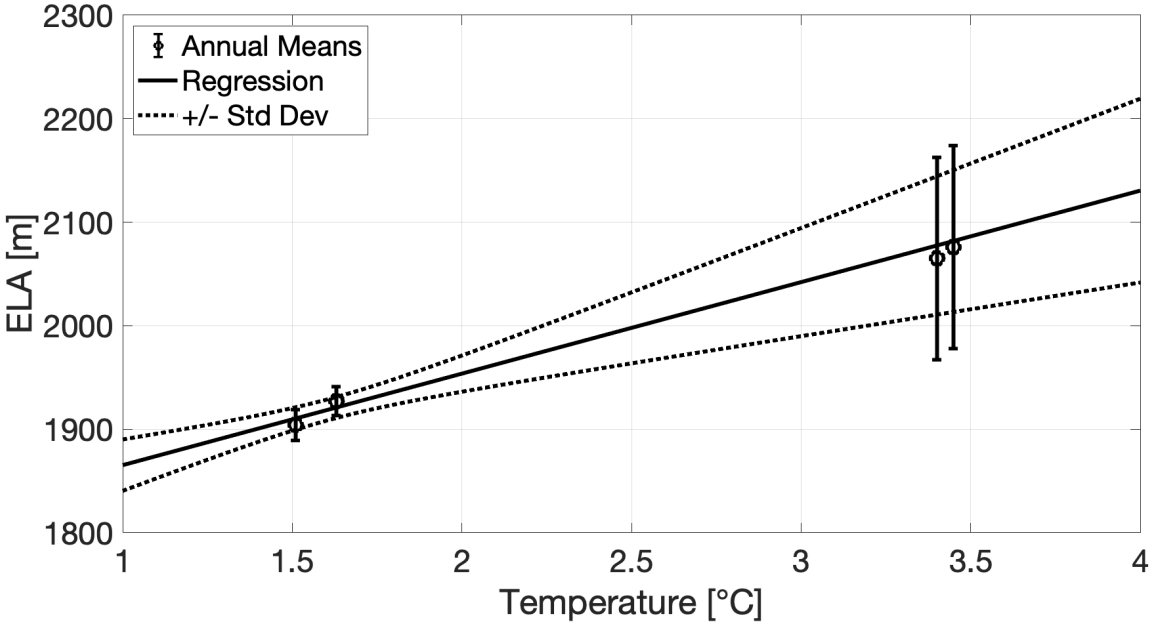

Figure 5. Relationship between annual temperature and ELA on Mocho-Choshuenco ice cap. The error bars indicate the error as estimated by Schaefer et al. (2017). The relationship between ELA and temperature was found through weighted linear regression.

In order to predict the ELA for any temperature, we first assume a linear relationship between both and solve a weighted least squares problem to find the slope and intercept (i.e. ELA gradient and ELA for 0°C). ELA predictions for any temperature $\{T_i, T_j, ...\}$ can be made by multiplying the forward operator $\hat{\mathbf{G}}$ with the vector $\mathbf{m}$ containing both model parameters:

$$\text{ELA} = \mathbf{Gm} = \mathbf{G}\mathcal{N}(\boldsymbol{\mu}, \boldsymbol{\Sigma}) = \mathcal{N}\left(\mathbf{G}\boldsymbol{\mu}, \mathbf{G}\boldsymbol{\Sigma}\mathbf{G}^T\right), \qquad \hat{\mathbf{G}} = \begin{pmatrix} T_i & 1 \\ T_j & 1 \\ \vdots & \vdots \end{pmatrix}. \tag{5}$$

$\mathbf{m}$ is distributed according to a bivariate normal distribution with mean vector $\boldsymbol{\mu}$ and model covariance matrix $\boldsymbol{\Sigma}$ (e.g. Aster et al., 2018):

$$\mathbf{m} \sim \mathcal{N}(\boldsymbol{\mu}, \boldsymbol{\Sigma}), \qquad \boldsymbol{\mu} = \left(\hat{\mathbf{G}}^T {\boldsymbol{\Sigma}_\mathbf{d}}^{-1} \hat{\mathbf{G}}\right)^{-1} \hat{\mathbf{G}}^T {\boldsymbol{\Sigma}_\mathbf{d}}^{-1} \hat{\mathbf{d}}, \qquad \boldsymbol{\Sigma} = \left(\hat{\mathbf{G}}^T {\boldsymbol{\Sigma}_\mathbf{d}}^{-1} \hat{\mathbf{G}}\right)^{-1}. \tag{6}$$

https://doi.org/10.5194/tc-2020-296
Preprint. Discussion started: 11 November 2020


The Cryosphere Discussions

Inserting the observed data, we identify the forward operator $\hat{\mathbf{G}}$, the data covariance matrix $\mathbf{\Sigma_d}$ and the vector of observed ELAs $\hat{\mathbf{d}}$ as

$$\hat{\mathbf{G}} = \begin{pmatrix} T_1 & 1 \\ T_2 & 1 \\ T_3 & 1 \\ T_4 & 1 \end{pmatrix}, \qquad \mathbf{\Sigma_d} = \begin{pmatrix} \sigma_1^2 & 0 & 0 & 0 \\ 0 & \sigma_2^2 & 0 & 0 \\ 0 & 0 & \sigma_3^2 & 0 \\ 0 & 0 & 0 & \sigma_4^2 \end{pmatrix}, \qquad \hat{\mathbf{d}} = \begin{pmatrix} \mathrm{ELA}_1 \\ \mathrm{ELA}_2 \\ \mathrm{ELA}_3 \\ \mathrm{ELA}_4 \end{pmatrix}. \tag{7}$$

Predictions for a general temperature T can be made through

$$\mathrm{ELA}(T) = \mathcal{N}\left(\mu_1 T + \mu_2,\ \Sigma_{11}T^2 + 2\Sigma_{12}T + \Sigma_{22}\right), \tag{8}$$

with

$$\boldsymbol{\mu} = \begin{pmatrix} 88\,\mathrm{m\,K^{-1}} \\ 1777\,\mathrm{m} \end{pmatrix}, \qquad \mathbf{\Sigma} = \begin{pmatrix} 1365\,\mathrm{m^2\,K^{-2}} & -2203\,\mathrm{m^2\,K^{-1}} \\ -2203\,\mathrm{m^2\,K^{-1}} & 3657\,\mathrm{m^2} \end{pmatrix}. \tag{9}$$

Figure 5 shows the mean of ELA predictions against temperature together with the ELA predictions of mean plus and minus one standard deviation.

Since the temperature projections give anomalies with respect to the period 2006-2020, we only rely on relative rather than absolute temperatures. Therefore, we convert the temperature changes into changes of ELA with the parameter $\mu_1 = 88\,\mathrm{m\,K^{-1}}$, which means that the ELA increases by 88 m per °C temperature increase. We assess the uncertainty propagation of this parameterization through the ice flow simulation code by performing additional experiments with upper and lower ELA gradients $\mu_1 \pm \sqrt{\Sigma_{11}} = (88 \pm 37)\,\mathrm{m\,K^{-1}}$ which corresponds to the one-sigma confidence interval.

3 Results

3.1 Spin-up and model calibration

First, we reproduce the present-day ice cap behaviour as a steady-state. We calculate the root mean square error for ice thickness difference between the observed and modelled ice caps. We update the mean ELA (B_{ELA}), ELA amplitude (A_{ELA}), maximum snowfall (S_0) and sliding coefficient (C_b) according to a Nelder-Mead algorithm (Nelder and Mead, 1965) to create an ensemble of parameter sets with similarly low root mean square error in ice thickness. Out of this ensemble, the set with best volume fit was chosen, with the final parameters being $B_{\mathrm{ELA}} = 2035\,\mathrm{m}$, $A_{\mathrm{ELA}} = 134\,\mathrm{m}$, $S_0 = 1.07\,\mathrm{m\,a^{-1}}$ and $C_b = 5.56 \cdot 10^{-5}\,\mathrm{m\,a^{-1}\,Pa^{-1}}$. We fixed the other parameters of the SMB parameterization to $M_0 = 0.023\,\mathrm{yr^{-1}}$ and $\varphi_0 = 315°$.

Figure 6a shows the volume evolution as the ice cap builds up under the chosen parameter set. Starting with zero ice, the simulation reaches an equilibrium state after 600 years with a volume close to the observed $1.038\,\mathrm{km^3}$ (Geoestudios, 2014). In

https://doi.org/10.5194/tc-2020-296
Preprint. Discussion started: 11 November 2020


The Cryosphere Discussions
Open Access
EGU

Figures 6b and 6c, the thickness distribution and thickness difference between modelled and observed ice caps are illustrated. Overall, a good agreement can be observed. Apart from local inaccuracies in ice thickness, there are two areas where the simulation does not reproduce well the observations: there is no ice between the two summits in the northern part of the ice cap, and a small ice tongue in the south-eastern catchment develops, with a maximum ice thickness of over $100\,\mathrm{m}$.

In Figure 6d, the ice flow velocity at the surface is shown. Overall, it rarely exceeds velocities of $30\,\mathrm{m\,yr^{-1}}$, with velocities towards the edges of the ice cap and in ice tongues being generally higher than on the plateau. On the eastern side of the ice cap, different catchments of outlet tongues can be identified. An outstanding feature is in the previously discussed south-eastern ice tongue where the ice velocity has a maximum of $200\,\mathrm{m\,yr^{-1}}$. The stakes where surface ice flow velocity observations are available are shown in Figure 6d, with the measured values indicated in Table 1. These are compared to simulated velocities at the stake locations, obtained through bilinear interpolation. While the velocities at stakes B10 and B12 are well represented, the simulated velocities at the other stakes are generally lower than the measured ones. However, they represent a yearly average, whereas the velocity measurements were taken in spring season, making a direct comparison difficult.

Stake	B8	B10	B12	B14	B15	B17	B18
v_{obs} $[\mathrm{m\,yr^{-1}}]$	22.2	12.7	60.3	33.8	19.4	31.2	27.2
v_{sim} $[\mathrm{m\,yr^{-1}}]$	11.5	12.4	60.1	18.4	14.4	9.6	11.2

Table 1. Comparison between simulated and observed velocities at stakes where velocity observations are available from Geoestudios (2013).

https://doi.org/10.5194/tc-2020-296
Preprint. Discussion started: 11 November 2020

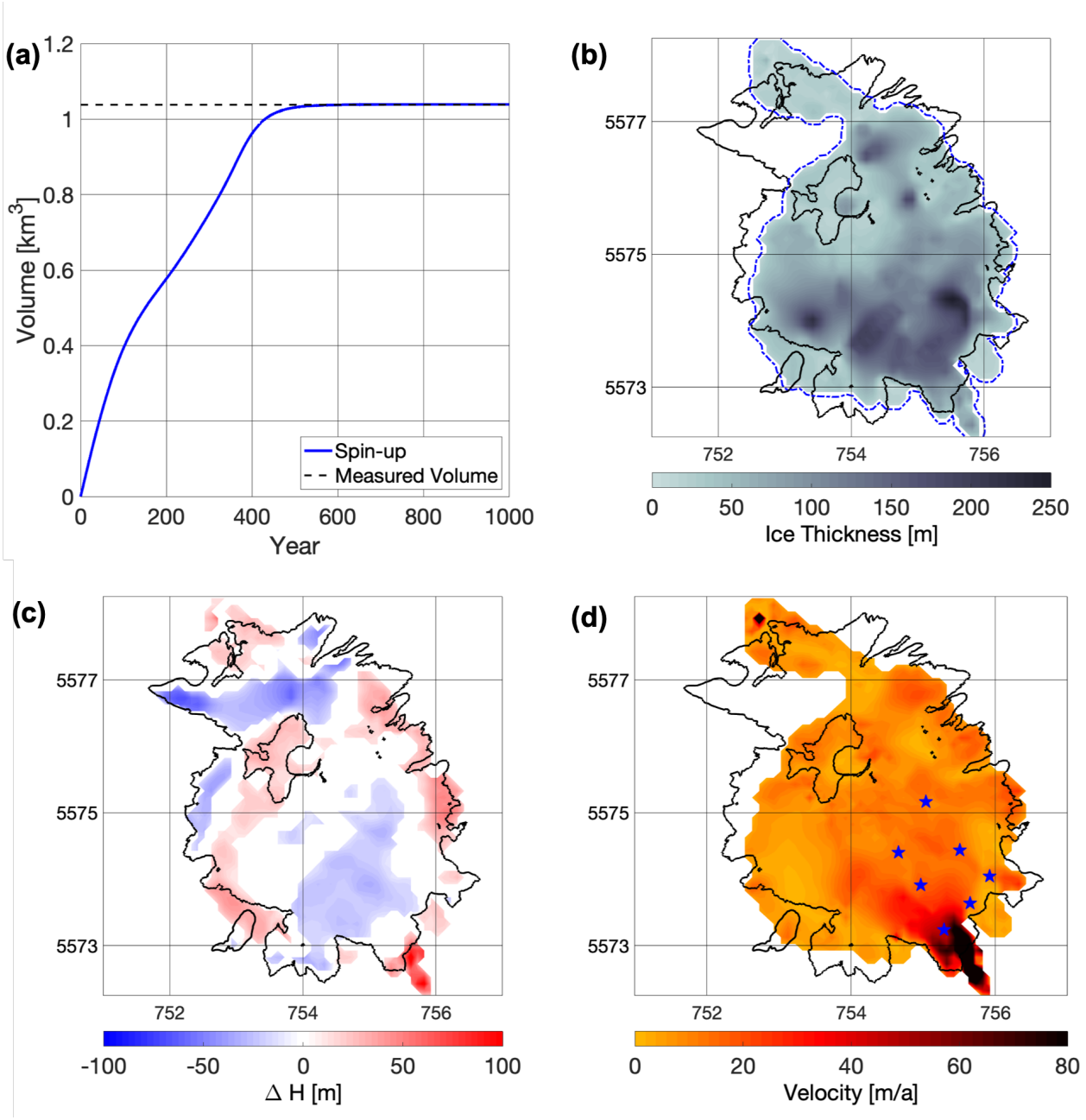

Figure 6. Results of the spin-up. (a) Volume evolution compared to observed volume, (b) Ice thickness distribution with observed (black) and modelled (blue) extent, (c) Difference between modelled and observed ice thickness, (d) Surface flow velocity and stakes with velocity observations.

https://doi.org/10.5194/tc-2020-296
Preprint. Discussion started: 11 November 2020

3.2 Projected ice thickness and area evolution

When forcing the ice cap with higher temperatures under the RCP2.6, RCP4.5 and RCP8.5 scenarios, the ice cap responds with an increase in its ELA. This increase, in turn, leads to thinning and retreat, i.e. to a lower ice thickness and a smaller ice area, respectively, towards the end of the century. Figure 7 shows the 21st century ice thickness evolution for the different scenarios, obtained after averaging through all 23 climate models for each of the three scenarios.

In the RCP2.6 scenario, thinning is more dominant than retreat. The ice retreats mostly in the northern part of the ice cap around the Choshuenco peak, and after 2060 in the outlet tongues of the southern part. Thinning, however, is ubiquitous and occurs over the whole domain during the 21st century.

The ice cap evolution under the RCP4.5 scenario shows a similar retreat pattern as that in RCP2.6, yet more areas in the southern part of the ice cap become ice free towards the end of the century. The most notable difference between the RCP4.5 and RCP2.6 is the higher abundance of thinning of the ice cap under the RCP4.5 scenario, particularly towards the end of the century.

The high-end scenario (RCP8.5) shows a clearly different pattern in both thinning and retreat over the 21st century. While the thickness pattern for 2040 is comparable to the two other scenarios, ice loss clearly accelerates in the second half of the century. This can be appreciated by the faint colors in the last two plots indicating an ice thickness of mostly under 100 m and a dramatic retreat until the year 2099.

Table 2 shows the maximum ice thickness in the same years obtained after averaging through all 23 climate models. The values confirm the observations taken from the thickness plots: thinning is present in all scenarios, but stronger in the RCP8.5 than in the other two scenarios. The uncertainty increases towards the end of the century, with the smallest growth rate in the RCP8.5 scenario where it even decreases in the last two decades of the 21st century.

https://doi.org/10.5194/tc-2020-296
Preprint. Discussion started: 11 November 2020

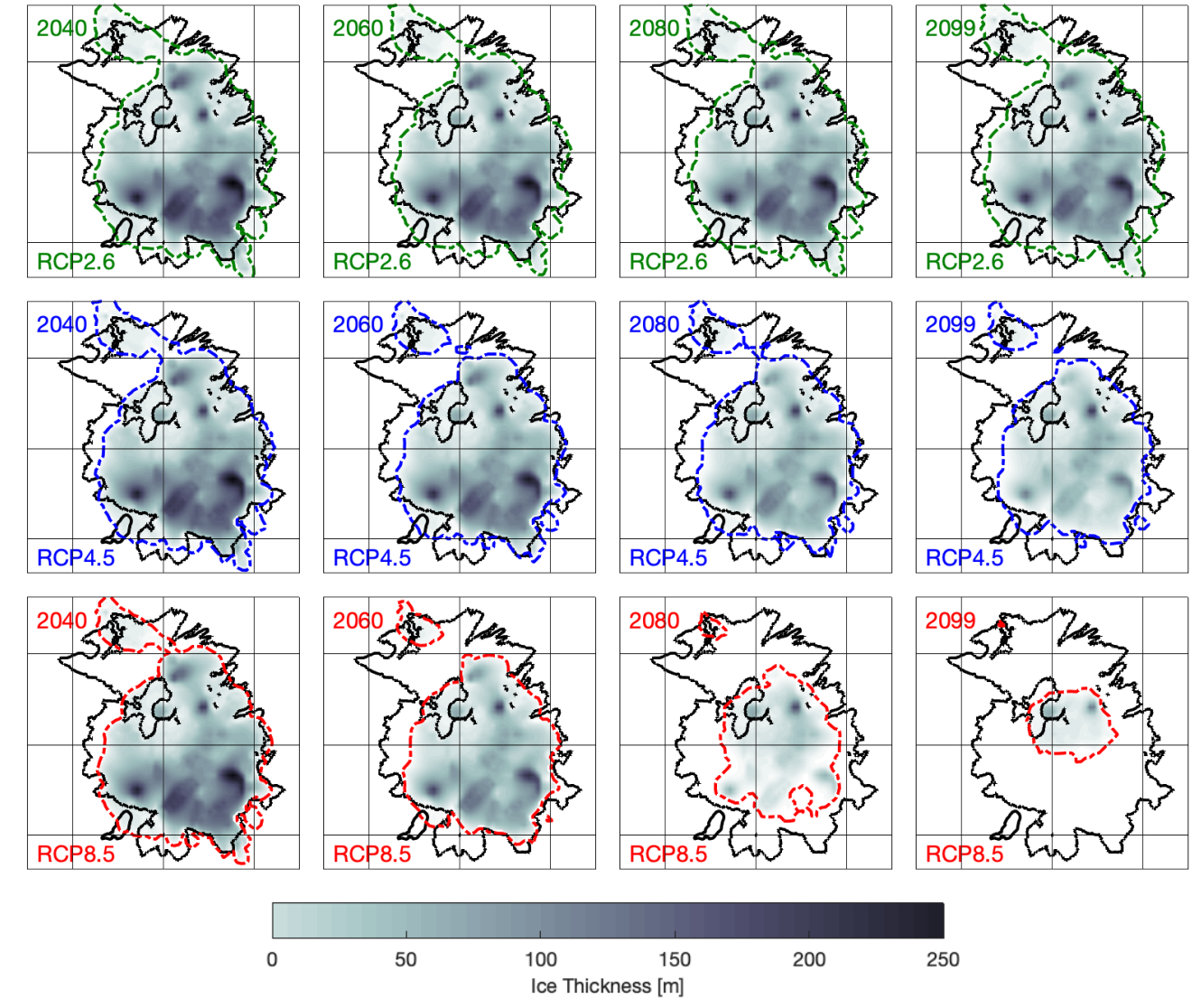

Figure 7. Ensemble mean ice thickness for three different future temperature scenarios and four different years, obtained by averaging the thickness obtained from all 23 climate models on every grid cell. The colored dashed lines show modeled ice extent, and black solid lines show the observed ice extent in 2013.

https://doi.org/10.5194/tc-2020-296
Preprint. Discussion started: 11 November 2020


The Cryosphere Discussions

Year	RCP2.6	RCP4.5	RCP8.5
2013	253.7	253.7	253.7
2040	244.6 ± 38.8	241.3 ± 21.8	236.9 ± 14.9
2060	234.8 ± 40.4	222.1 ± 34.2	194.6 ± 22.7
2080	224.9 ± 54.8	186.5 ± 56.6	166.7 ± 46.6
2099	214.9 ± 74.4	178.4 ± 82.1	122.7 ± 34.7

Table 2. Projected maximum ice thickness in meters for different scenarios and years: mean and standard deviation obtained by forcing SICOPOLIS for 23 climate models.

3.3 Projected ice volume evolution

Projected thinning and retreat of the ice cap illustrated in the previous Section yield the loss in total ice volume. The evolution of the total ice volume under different scenarios is shown in Figure 8. The projections for the 23 individual climate models (thin lines) can be summarized by the multimodel ensemble mean (thick solid lines) and one-sigma confidence interval (thick dashed lines). The three scenarios begin to diverge in the 2040s, and in the 2050s the glacier projections obtained with the RCP8.5 scenario start to clearly diverge from the other two scenarios. The ice volume evolution under the RCP2.6 and RCP4.5 scenarios shows similar behaviour until the mid century, whereas notable differences exist between them towards the end of the century, particularly after the 2080s.

There is a large agreement among the ensemble members of the RCP8.5 scenario that generally show the same declining patterns, which are even more prominent by the end of the century. On the other hand, RCP4.5 and RCP2.6 scenarios show increase in uncertainty with the increase in time, in particular, the projections under the RCP2.6 scenario illustrate a large uncertainty bound spanning from the mid century to the end of the century. These contrasts in the projections under different emission scenarios reflect higher signal-to-noise ratio for the RCP8.5 scenario, as this scenario has a more prominent temperature increase (also see Figure 4). It is worth noting that ice volume evolution tends to have similar changes with a small uncertainty bound under each scenario during the first two decades (i.e., until 2040s) which can be explained by the dominant role of the internal variability in the near future. Projected ice volumes for different scenarios and years are summarized in Table 3.

https://doi.org/10.5194/tc-2020-296
Preprint. Discussion started: 11 November 2020

The Cryosphere Discussions
Open Access
EGU

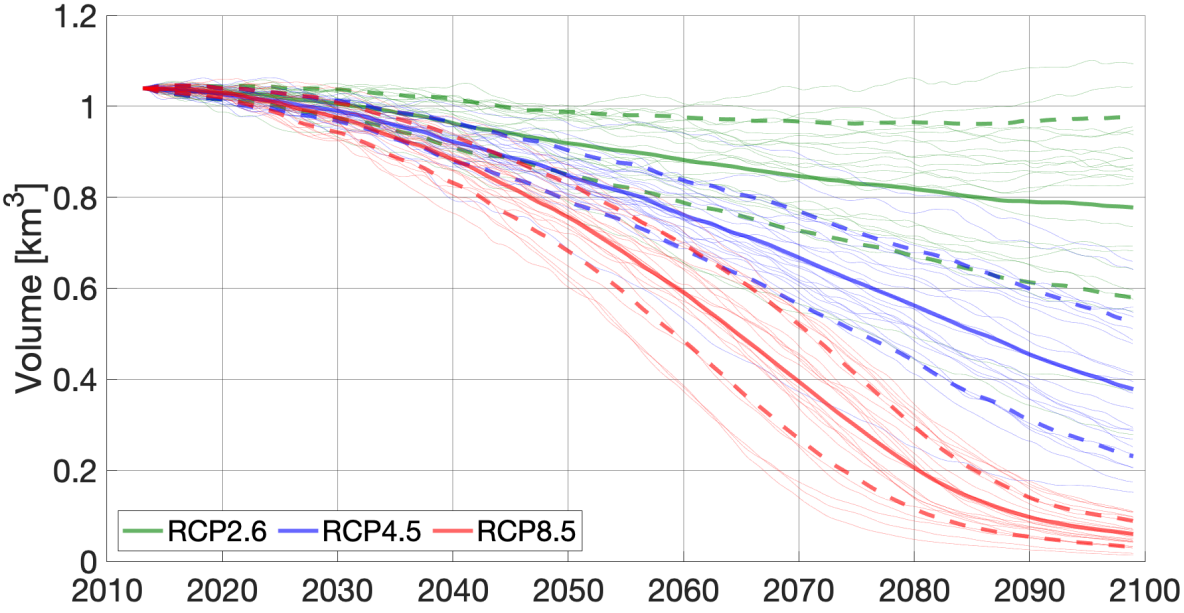

Figure 8. Ice volume evolution under the three scenarios RCP2.6 (green), RCP4.5 (blue) and RCP8.5 (red) until the year 2100. Thin lines show the 23 individual evolutions from different climate models, thick solid lines indicate their mean and thick dashed lines the mean plus/minus standard deviation.

Year	RCP2.6	RCP4.5	RCP8.5
2013	1.04	1.04	1.04
2040	0.93 ± 0.05	0.88 ± 0.04	0.85 ± 0.05
2060	0.84 ± 0.09	0.73 ± 0.07	0.57 ± 0.1
2080	0.79 ± 0.14	0.54 ± 0.11	0.2 ± 0.09
2099	0.75 ± 0.19	0.36 ± 0.14	0.06 ± 0.03

Table 3. Projected ice volumes in km^3 for different scenarios and years: mean and standard deviation obtained by forcing SICOPOLIS for 23 climate models.

3.4 Uncertainty of ELA gradient

220 In this Section, we analyse the impact that the ELA dependence on temperature has on glacier projections. We average the 23 climate model temperature projections for the three scenarios before running SICOPOLIS instead of forcing it individually with each climate model as in the previous sections. With these mean projections, we perform three model runs for each scenario: the mean gradient between temperature and ELA ($88\,\mathrm{m\,K^{-1}}$), and the upper and lower bound of the one-sigma confidence

https://doi.org/10.5194/tc-2020-296
Preprint. Discussion started: 11 November 2020

interval ($51\,\mathrm{m\,K^{-1}}$ and $125\,\mathrm{m\,K^{-1}}$). The resulting ice volume evolutions are shown in Figure 9, with the mean in solid lines and the one-sigma confidence interval indicated by dashed lines.

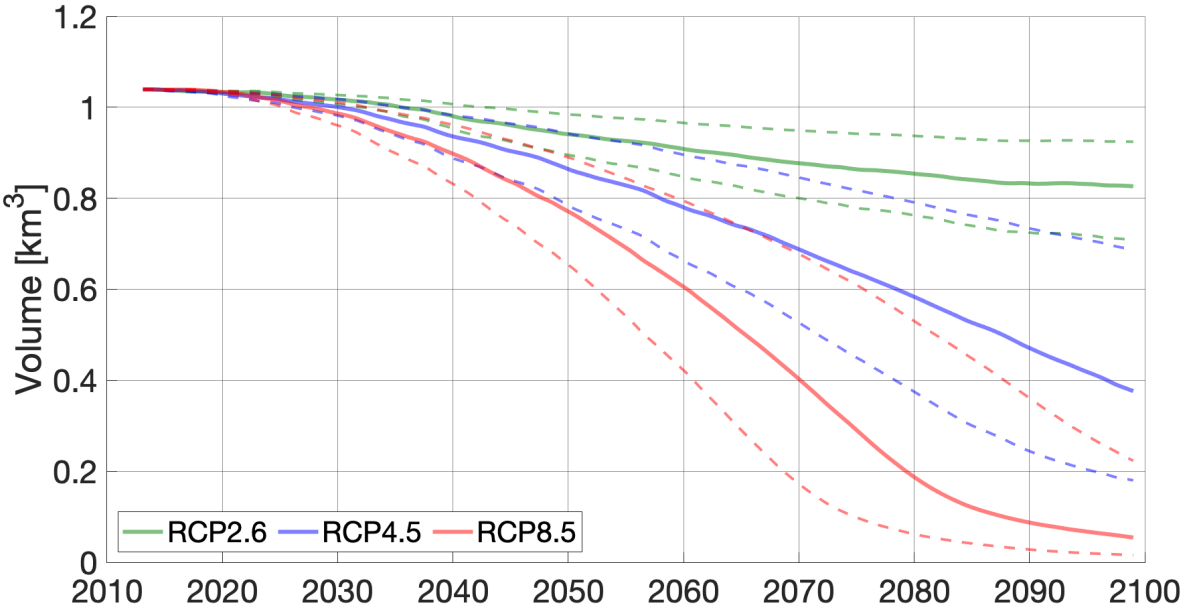

Figure 9. Volume evolution for different gradients between ELA and temperature.

https://doi.org/10.5194/tc-2020-296
Preprint. Discussion started: 11 November 2020

4 Discussion

4.1 Present-day simulations

The first part of our study consists of the creation of a present-day steady-state of the Mocho-Choshuenco ice cap. Since drivers of the SMB such as solar radiation and snow redistribution are strongly aspect-dependent, we developed a new SMB parameterization accounting for aspect-dependent SMB variations (see Section 2.3). As shown in Figure 6a, the steady-state now reaches a volume very similar to the observed one, and the ice thickness distribution and ice outline (Figure 6b) match the observations much better than previously, without the new parameterization (Flández, 2017). Also, the simulated velocities are mostly in good agreement with observed values (see Figure 6d and Table 1).

The difference between observed and simulated thickness (Figure 6c) shows over- and underestimations of up to 100 m, with two notable features. In the south-eastern part of the ice cap, the simulations create a new ice tongue. This feature can be explained by high ice velocities in this area (Figure 6d), leading to a fast redistribution of ice before the highly negative SMB melts it away. However, close observations of satellite images show that there is a debris-covered body of dead ice in the valley below the glacier (Scheiter, 2019). This shows that the persistence of ice in this area is not unrealistic, even though the high observed velocities demonstrate that ice dynamics are not well represented by our model (Figure 6d).

The other notable feature is the area between the two summits where no ice is present in the simulations, contradicting the observations. One possible explanation is that the SMB variations underlying our aspect-dependent SMB parameterization also hold for the Choshuenco peak, but were only applied to the Mocho peak. Furthermore, there are no GPR data available in this area (see Figure 2b), making an interpretation difficult in the context of this study.

The velocities presented in Table 1 show simulated values at the stake locations that are lower than the observed ones. However, a direct comparison is not meaningful as the observed values were taken in October, while the simulated velocities are representative for the whole year. Furthermore, the flow exponent $n = 3$ in Glen's flow law leads to a significant underestimation of surface velocities where thickness is also underestimated. Most stakes lie in areas where the ice is thicker in simulations than in observations (see Figures 6c and 6d), making this a reasonable explanation. On several stakes (B10, B12, B15), the velocities are well matched, and we conclude that our spin-up reproduces the observed ice cap well, considering the given observations.

4.2 21st century projections

For the RCP2.6 scenario, we project a steady decay in ice volume until the end of the 21st century. This ice loss is predominantly driven by thinning, and to a lesser degree by retreat. A reason for this might be that the ice cap is in an overall stable position at the moment and slow temperature increase leads first to thinning and then to retreat due to dynamical glacier response. We assess the uncertainty of the RCP2.6 scenario based on two influences: different climate models and the uncertainty of the ELA against temperature parameterization. Both uncertainties increase linearly over the 21st century, but the climate ensemble uncertainty has about twice the magnitude. A possible explanation for this is that the moderate average increase in temperature of only $0.33°\mathrm{C}$ does not emphasize differences in the ELA gradient as much as it is the case for more drastic scenarios.

https://doi.org/10.5194/tc-2020-296
Preprint. Discussion started: 11 November 2020

In the RCP4.5 scenario, our projections show a higher retreat rate compared to the RCP2.6 scenario, and together with a relatively high thinning rate in the end of the 21st century leads, the ice loss almost doubles. Similar to the previous scenario, the RCP4.5 projections also shows a linear, but slightly slower increase in climate model uncertainty, separating significantly from the RCP2.6 scenario in the 2080s. The uncertainty introduced by the ELA gradient variations is much higher than in the RCP2.6 scenario. This underpins the conclusion that the higher rate in temperature increase emphasizes the ELA gradient differences more.

The high-end atmospheric warming scenario RCP8.5 causes a highly accelerated ice loss from the 2040s to the 2080s with high retreat rates, before becoming more subtle from 2080 to 2100. This behaviour illustrates a highly unstable ice cap during most of the 21st century, and the more subtle retreat in the 2090s can be explained by the fact that most ice has already melted away. This saturation in volume loss can also be observed in the climate model uncertainty: while it increases strongly between 2050 and 2080, it becomes very small towards the end of the century, showing an overall agreement between the climate models regarding the point in time where the ice cap almost vanishes. The ELA uncertainty shows a similar behaviour, with an increase until 2080 and subsequent decrease, which is more pronounced for the lower bound. The ice loss for the upper bound remains lower than that in the lower bound of the RCP4.5 scenario, which highlights the high uncertainty introduced by the ELA parameterization.

4.3 Limitations of our approach

In this study, the principal uncertainties we assign to our results are based on the spread of the temperature projections of the global circulation models and on the uncertainty of the temperature-ELA parameterization. In this section, we discuss possible further sources of uncertainty, and make suggestions on how future work could encounter these challenges.

Our approach is based on the shallow ice approximation (SIA), with assumptions including almost parallel and horizontal glacier bed and surface, significantly larger horizontal than vertical dimensions and simple-shear ice deformation. While these assumptions hold well for the large Greenlandic and Antarctic ice sheets, it is less obvious that the SIA can be employed on such a small study object as the Mocho-Choshuenco ice cap. The SIA assumptions are violated especially in the steep regions around the two summits and towards the boundaries of the present-day ice cap. However, they hold true for large parts of the plateau on the south-eastern part which accounts for over a third of the ice cap and most important area in our future projections. Previous studies have suggested that low-order assumptions such as the SIA hold well for glaciers whose behaviours are mostly driven by SMB (Adhikari and Marshall, 2013), which is the case for the Mocho-Choshuenco ice cap. However, it would be a valuable experiment to reproduce our results with a full-Stokes model such as Elmer/Ice to verify the applicability of the SIA.

Knowledge about the bed of the ice cap is essential to perform ice flow simulations. We created a bed map based on present-day topography and a number of ground-penetrating radar profiles published by Geoestudios (2014). Even though these profiles cover a significant portion of the ice cap, there are large gaps in data coverage, especially in the north-eastern part of the ice cap. More observations could help to reduce the uncertainty introduced by these gaps.

Regarding the ELA gradient we use to relate temperature increase to glacier response, it is important to note that we have a few data points given for this relationship (Schaefer et al., 2017). With more years of ELA-temperature pairs and a thorough

https://doi.org/10.5194/tc-2020-296
Preprint. Discussion started: 11 November 2020

uncertainty estimation, we could achieve a higher confidence in our ELA gradient. However, by performing the simulations for the mean gradient and a lower and upper bound, we are within the range of most previous studies (e.g. Six and Vincent, 2014; Sagredo et al., 2014; Wang et al., 2019).

Another significant limitation lies in the SMB parameterization. While the new aspect-dependent parameterization was able to improve the reproduction of the present-day ice cap significantly, there is still space for improvement. Especially the northern part is still not well reproduced by SICOPOLIS, and it might be of advantage to extend the new parameterization to the Choshuenco peak. In order to verify our parameterization, it would be helpful to obtain SMB measurements in the north-west, i.e. between both summits, and thus extend the stake network that is currently focused on the main catchment in the south-east of Mocho summit. This could provide more observational constraints on the ELA difference between the north-west and south-east.

Another way of producing more realistic SMB maps for the ice cap would be using explicit models that try to quantify the physical processes which determine glacier mass balance, e.g. the COSIPY Model (Sauter et al., 2020). Drawbacks of these complex models is that they need many input parameters (such as precipitation, relative humidity or wind speed) with a high spatial resolution. These can be obtained by regional climate model simulations (e.g. Bozkurt et al., 2019). However considerable uncertainties are associated to these simulations and a careful validation of the results is necessary before using them as drivers of SMB simulations. Additionally, only few high resolution regional climate simulations are available in the moment which is why we prefer our simple temperature dependent SMB parameterization combined with a multi-model approach using 23 different GCMs as drivers of our simulations.

4.4 Global context of glacier decline

To our knowledge, there are only few previous studies that have projected the future evolution of glaciers in the Andes. The nearest study object to the Mocho-Choshuenco ice cap is the Northern Patagonian Icefield for which until 2100 an ice mass loss of 592 Gt has been projected under the A1B scenario which is comparable to the RCP6.0 scenario, and therefore between our results for RCP4.5 and RCP8.5 (Schaefer et al., 2013). Relating this ice loss to more recent estimates of total ice mass (Carrivick et al., 2016; Millan et al., 2019), around 50% of the ice mass would have disappeared. However, these simulations were performed on a fixed geometry, and therefore considered only changes in SMB, making it difficult to compare their results to ours. Collao-Barrios et al. (2018) obtained a committed mass loss of approximately 10% for San Rafael Glacier under current climate. However, they also maintained glacier area constant during their simulations and therefore neglect glacier retreat, which could dramatically change rates of frontal ablation.

Möller and Schneider (2010) projected the future evolution of Glaciar Noroeste, an outlet glacier of the Gran Campo Nevado ice cap in southern Patagonia between 1984 and 2100. Their projections were made for the B1 scenario and yielded a volume loss of around 45% which is significantly less than the 61% volume loss that we project for the comparable RCP4.5 scenario between 2013 and 2100. Their results are based on a calibrated relationship between area and volume, and not on ice flow modelling as our study.

https://doi.org/10.5194/tc-2020-296
Preprint. Discussion started: 11 November 2020

The only ice sheet modelling approach to project future change under climate change scenarios in the Andes so far is the work of Réveillet et al. (2015) on Zongo glacier in Bolivia, using the full-Stokes model Elmer/Ice. They projected 40% and 89% volume loss for the RCP2.6 and RCP8.5 scenarios, respectively. The value for the high-end scenario is comparable to ours (94%), which might be expected as both glaciers are about to disappear by the end of the century, and therefore have already lost the majority of their ice mass. On the other hand, our projections for the RCP2.6 are lower (25%) than their RCP2.6 projections. The might be due to the climate differences between the tropics and the Wet Andes, and also due to the higher ELA gradient with temperature of $150\,\mathrm{m\,K^{-1}}$ used in their study in comparison to $88\,\mathrm{m\,K^{-1}}$ used in our study.

Hock et al. (2019) projected future mass loss in 19 different glacier regions worldwide using six different glacier models of different complexity. Similar to our approach, different ensemble of the CMIP5 GCMs were used to drive the glacier model projections. For the Southern Andes, they projected regional ice mass losses of 18.7% (RCP2.6), 31.6% (RCP4.5) and 45.6% (RCP8.5). Their projected regional percental mass losses are clearly lower than our projected mass loss for the Mocho-Choshuenco ice cap, especially for RCP4.5 and RCP8.5. Here it is important to note that the regional mass loss in the Southern Andes is greatly determined by the mass loss of the large Patagonian ice fields. Here many glaciers are calving glaciers and the projections of Hock et al. (2019) need to be interpreted with care, since only one of the six models include a parameterization of frontal ablation.

Outside of South America, there are several studies that project a glacier shrinkage similar to our projections in the next 100 years. Kienholz et al. (2017) projected a mass loss of 73% for Black Rapids Glacier in Alaska between 1980 and 2100 under the RCP8.5 scenario with a SMB model coupled to a simple mass-conservation based retreat parameterization. They used a similar downscaling approach to obtain high-resolution temperature and precipitation fields than that applied by Schaefer et al. (2013).

Another study in North America is that of Adhikari and Marshall (2013) who performed ice flow simulations on Haig Glacier in the Rocky Mountains and projected the disappearance of the glacier by 2080 under the RCP4.5 and RCP8.5 scenarios. These results hold for both high-order and low-order mechanical models, and the authors conclude that low-order models are suitable for glaciers with low ice velocity and a glacier geometry controlled largely by SMB. As these conditions hold strongly for the Mocho-Choshuenco ice cap, their conclusions also underpin our assumption that a low-order model such as SICOPOLIS is sufficient to simulate the ice dynamics of our ice cap.

Other studies conducted on glaciers in Europe show similar results as ours: Jouvet et al. (2011) projected a volume loss of 90% for Grosser Aletschgletscher in Switzerland until 2100 under the A1B scenario, and indicated that even under the present climate the glacier is in disequilibrium and would continue to lose significant amounts of ice.

Wang et al. (2019) investigated the future evolution of Austre Lovénbreen with the full-Stokes ice flow model Elmer/Ice, a mountain glacier in Svalbard, and found that with an intermediate temperature increase scenario the glacier would disappear by 2120, and by 2093 for the most pessimistic scenario

Even though different model setups and parameterizations were applied for all glaciers in the mentioned studies, most of them show a similar trajectory for the glacier evolution in the next 60 to 100 years, and our projections for the Mocho-Choshuenco ice cap fit well into them. All of them lose a high percentage of ice mass during the 21st century and we can expect

https://doi.org/10.5194/tc-2020-296
Preprint. Discussion started: 11 November 2020

many mountain glaciers in different parts of the world to disappear in the first half of the 22nd century, without reductions of greenhouse gases.

5 Conclusions

In this study, we applied the ice sheet model SICOPOLIS to reproduce the current state of the Mocho-Choshuenco ice cap and to project its future evolution under different emission scenarios. This is the first estimate of future glacier evolution obtained from a flow model in the Wet Andes, and one of the first in the whole Andes. Using a linear temperature-ELA parameterization, we investigate the future of the ice cap using projected temperature changes from 23 GCMs as input. A considerable spread of the projected ice volume at the end of the 21st century is obtained, depending on the emission scenario and GCM. However, under the emission scenario RCP8.5, which does not consider a reduction of our emission of greenhouse gases, the spread of the results is less pronounced and in this scenario it is likely that the ice cap will loose more then 90% of it current volume by 2100. Since temperature projections are relatively uniform in the region and geometry of the surrounding ice caps are similar to Mocho-Choshuenco ice cap, we project similar high volume losses for other ice-caps in the Chilean Lake District (39-41.5°S).

The Mocho-Choshuenco ice cap is the smallest ice body to which SICOPOLIS has been applied so far, justified a priori by the cap-like geometry (as opposed to, for example, valley glaciers), and a posteriori by the reasonably good performance of the model in replicating the present-day ice cap. Nevertheless, it would be valuable to check if the application of a full-Stokes glacier flow model (as for example Elmer/Ice, Gagliardini et al. (2013)) affected the simulated state of the ice cap notably, or if the disagreements are mainly caused by our simplified surface mass balance parameterization. When projecting the future of the large Patagonian icefields in the southern part of the Wet Andes, the interaction of their outlet glaciers with the surrounding water bodies becomes crucial. Adequate parameterizations for frontal ablation are necessary, which allow the glaciers to adapt their frontal positions according to the glacier flow, which will be crucially determined by these parameterizations.

https://doi.org/10.5194/tc-2020-296
Preprint. Discussion started: 11 November 2020


The Cryosphere Discussions
Open Access
EGU

Appendix A: Global climate models

Table A1 gives details on the 23 global climate models that were used to force SICOPOLIS with future temperature projections.

IPCC Model ID	Institution	Resolution (degree) (LonxLat)
BCC_CSM1_1	Beijing Climate Center, China Meteorological Administration, China	2.81x2.77
BCC_CSM1_1_M		1.12x1.12
BNU_ESM	College of Global Change and Earth System Science, Beijing Normal University, China	2.8x2.8
CanESM2	Canadian Centre for Climate Modelling and Analysis, Canada	2.81x2.79
CCSM4	National Center of Atmospheric Research, USA	1.25x0.94
CESM1-CAM5		1.25x0.94
CNRM_CM5	National Center of Meteorological Research, France	1.41x1.40
CSIRO_Mk3_6_0	Commonwealth Scientific and Industrial Research Organization (CSIRO), Australia	1.875x1.86
FIO_ESM	The First Institute of Oceanography, SOA, China	2.8x2.8
GFDL_CM3	NAOO Geophysical Fluid Dynamics Laboratory, USA	2.5x2.0
GFDL_ESM2G		2.5x2.0
GFDL_ESM2M		2.5x2.0
GISS-E2-H	Goddard Institute for Space Studies, USA	2.5x2.0
GISS-E2-R		2.5x2.0
HadGEM2-AO	Met Office Hadley Centre, UK	1.875x1.25
IPSL-CM5A-MR	Institut Pierre-Simon Laplace, France	2.5x1.25
MIROC5	Atmosphere and Ocean Research Institute (The University of Tokyo), National Institute for Environmental Studies and Japan Agency for Marine-Earth Science and Technology, Japan	1.41x1.39
MIROC_ESM		2.81x1.77
MIROC_ESM_CHEM		2.81x1.77
MPI_ESM_LR	Max Planck Institute for Meteorology, Germany	1.875x1.85
MPI_ESM_MR		1.875x1.85
MRI_CGCM3	Meteorological Research Institute, Japan	1.125x1.125
NorESM1_M	Norwegian Climate Center, Norway	2.5x1.875

Table A1. Details of global climate models used in this study. For further information on CMIP5 and the individual models, see Taylor et al. (2012) and references therein.

https://doi.org/10.5194/tc-2020-296
Preprint. Discussion started: 11 November 2020

Author contributions. Marius Schaefer, Ralf Greve, and Matthias Scheiter designed the study. Ralf Greve developed the ice-sheet model SICOPOLIS. Matthias Scheiter ran the simulations with advice from Marius Schaefer and Ralf Greve. Eduardo Flández contributed to the simulations. Deniz Bozkurt provided the temperature projection data and assisted with the ice cap projections. Matthias Scheiter wrote the manuscript with contributions from all authors. All authors discussed and interpreted the results.

Competing interests. The authors declare that no competing interests are present.

Acknowledgements. We thank Gino Casassa for providing the ice thickness data used in this study. We are grateful to Andrew Valentine, Buse Turunçtur, and Shubham Agrawal for discussions that helped to improve this paper, and to Klaus Spitzer and Malcolm Sambridge for their generous support in undertaking this research. We acknowledge the World Climate Research Programme Working Group on Coupled Modelling, which is responsible for CMIP, and we thank the climate modeling groups (listed in Table A1) for producing and making available their model output. Matthias Scheiter acknowledges financial support from the Australian National University and the CSIRO Deep Earth Imaging Future Science Platform. Marius Schaefer is supported by the FONDECYT Regular Grant, Etapa 2018, grant no. 1180785. Eduardo Flández acknowledges support from FONDECYT grant no. 1201967. Deniz Bozkurt acknowledges support from CONICYT-PAI 77190080 and ANID-PIA-Anillo INACH ACT192057. Ralf Greve was supported by Japan Society for the Promotion of Science (JSPS) KAKENHI grant Nos. JP16H02224, JP17H06104 and JP17H06323, by a Leadership Research Grant of Hokkaido University's Institute of Low Temperature Science (ILTS), and by the Arctic Challenge for Sustainability projects ArCS and ArCS II of the Japanese Ministry of Education, Culture, Sports, Science and Technology (MEXT) (program grant number JPMXD1300000000).

https://doi.org/10.5194/tc-2020-296
Preprint. Discussion started: 11 November 2020

References

Adhikari, S. and Marshall, S.: Influence of high-order mechanics on simulation of glacier response to climate change: insights from Haig Glacier, Canadian Rocky Mountains., Cryosphere, 7, https://doi.org/10.5194/tc-7-1527-2013, 2013.

Aster, R. C., Borchers, B., and Thurber, C. H.: Parameter estimation and inverse problems, Elsevier, 2018.

Bernales, J., Rogozhina, I., Greve, R., and Thomas, M.: Comparison of hybrid schemes for the combination of shallow approximations in numerical simulations of the Antarctic Ice Sheet, Cryosphere, 11, 247–265, https://doi.org/10.5194/tc-11-247-2017, 2017.

Blatter, H. and Greve, R.: Comparison and verification of enthalpy schemes for polythermal glaciers and ice sheets with a one-dimensional model, Polar Sci., 9, 196–207, https://doi.org/10.1016/j.polar.2015.04.001, 2015.

Bozkurt, D., Rojas, M., Boisier, J. P., Rondanelli, R., Garreaud, R., and Gallardo, L.: Dynamical downscaling over the complex terrain of southwest South America: present climate conditions and added value analysis, Clim. Dyn., 53, 6745–6767, https://doi.org/10.1007/s00382-019-04959-y, 2019.

Braun, M. H., Malz, P., Sommer, C., Farías-Barahona, D., Sauter, T., Casassa, G., Soruco, A., Skvarca, P., and Seehaus, T. C.: Constraining glacier elevation and mass changes in South America, Nat. Clim. Change, p. 1, https://doi.org/10.1038/s41558-018-0375-7, 2019.

Calov, R., Beyer, S., Greve, R., Beckmann, J., Willeit, M., Kleiner, T., Rückamp, M., Humbert, A., and Ganopolski, A.: Simulation of the future sea level contribution of Greenland with a new glacial system model, Cryosphere, 12, 3097–3121, https://doi.org/10.5194/tc-12-3097-2018, 2018.

Carrivick, J. L., Davies, B. J., James, W. H., Quincey, D. J., and Glasser, N. F.: Distributed ice thickness and glacier volume in southern South America, Glob. Planet. Change, 146, 122 – 132, https://doi.org/10.1016/j.gloplacha.2016.09.010, 2016.

Collao-Barrios, G., Gillet-Chaulet, F., Favier, V., Casassa, G., Berthier, E., Dussaillant, I., Mouginot, J., and Rignot, E.: Ice flow modelling to constrain the surface mass balance and ice discharge of San Rafael Glacier, Northern Patagonia Icefield, J. Glaciol., 64, 568–582, https://doi.org/10.1017/jog.2018.46, 2018.

Cuffey, K. M. and Paterson, W. S. B.: The Physics of Glaciers, Elsevier, Amsterdam, The Netherlands etc., 4th edn., 2010.

Dunse, T., Greve, R., Schuler, T. V., and Hagen, J. O.: Permanent fast flow versus cyclic surge behaviour: numerical simulations of the Austfonna ice cap, Svalbard, J. Glaciol, 57, 247–259, https://doi.org/10.3189/002214311796405979, 2011.

Dussaillant, I., Berthier, E., Brun, F., Masiokas, M., Hugonnet, R., Favier, V., Rabatel, A., Pitte, P., and Ruiz, L.: Two decades of glacier mass loss along the Andes, Nat. Geosci, 12, 802–808, https://doi.org/10.1038/s41561-019-0432-5, 2019.

Flández, E.: Modelamiento Numérico de la Dinámica de la Capa de Hielo Mocho-Choshuenco, Seminario de Graduacion, Universidad Austral de Chile, 2017.

Gagliardini, O., Zwinger, T., Gillet-Chaulet, F., Durand, G., Favier, L., de Fleurian, B., Greve, R., Malinen, M., Martín, C., Råback, P., Ruokolainen, J., Sacchettini, M., Schäfer, M., Seddik, H., and Thies, J.: Capabilities and performance of Elmer/Ice, a new-generation ice sheet model, Geosci. Model Dev., 6, 1299–1318, https://doi.org/10.5194/gmd-6-1299-2013, https://gmd.copernicus.org/articles/6/1299/2013/, 2013.

Garreaud, R., Lopez, P., Minvielle, M., and Rojas, M.: Large-Scale Control on the Patagonian Climate, J. Clim, 26, 215–230, https://doi.org/10.1175/JCLI-D-12-00001.1, 2013.

Geoestudios: Implementación nivel 2 estrategia nacional de glaciares: mediciones glaciológicas terrestres en Chile central, zona sur y Patagonia, Tech. rep., Dirección General de Aguas, S.I.T. No. 327, 2013.

https://doi.org/10.5194/tc-2020-296
Preprint. Discussion started: 11 November 2020

Geoestudios: Estimación de volúmenes de hielo: sondajes de radar en zonas norte, central y sur, Tech. rep., Dirección General de Aguas, S.I.T. No. 338, https://snia.mop.gob.cl/sad/GLA5504_informe_final.pdf, 2014.

Greve, R.: A continuum-mechanical formulation for shallow polythermal ice sheets, Phil. Trans. R. Soc. A, 355, 921–974, https://doi.org/10.1098/rsta.1997.0050, 1997a.

Greve, R.: Application of a polythermal three-dimensional ice sheet model to the Greenland ice sheet: Response to steady-state and transient climate scenarios, J. Climate, 10, 901–918, https://doi.org/10.1175/1520-0442(1997)010<0901:AOAPTD>2.0.CO;2, 1997b.

Greve, R. and Blatter, H.: Comparison of thermodynamics solvers in the polythermal ice sheet model SICOPOLIS, Polar Sci., 10, 11–23, https://doi.org/10.1016/j.polar.2015.12.004, 2016.

Greve, R. and SICOPOLIS Developer Team: SICOPOLIS v5.1, Zenodo, https://doi.org/10.5281/zenodo.3727511, 2019.

Hock, R., Bliss, A., Marzeion, B., Giesen, R. H., Hirabayashi, Y., Huss, M., Radić, V., and Slangen, A. B.: GlacierMIP–A model intercomparison of global-scale glacier mass-balance models and projections, J. Glaciol., 65, 453–467, https://doi.org/10.1017/jog.2019.22, 2019.

IPCC: Summary for Policymakers, in: Climate Change 2013: The Physical Science Basis. Contribution of Working Group I to the Fifth Assessment Report of the Intergovernmental Panel on Climate Change, edited by Stocker, T. F., Qin, D., Plattner, G.-K., Tignor, M., Allen, S. K., Boschung, J., Nauels, A., Xia, Y., Bex, V., and Midgley, P. M., pp. 3–29, Cambridge University Press, Cambridge, UK and New York, NY, USA, 2013.

Jouvet, G., Huss, M., Funk, M., and Blatter, H.: Modelling the retreat of Grosser Aletschgletscher, Switzerland, in a changing climate, J. Glaciol, 57, 1033–1045, https://doi.org/10.3189/002214311798843359, 2011.

Kienholz, C., Hock, R., Truffer, M., Bieniek, P., and Lader, R.: Mass balance evolution of black rapids glacier, Alaska, 1980–2100, and its implications for surge recurrence, Front. Earth Sci., 5, 56, https://doi.org/10.3389/feart.2017.00056, 2017.

Millan, R., Rignot, E., Rivera, A., Martineau, V., Mouginot, J., Zamora, R., Uribe, J., Lenzano, G., De Fleurian, B., Li, X., Gim, Y., and Kirchner, D.: Ice Thickness and Bed Elevation of the Northern and Southern Patagonian Icefields, Geophys. Res. Lett., 46, 6626–6635, https://doi.org/10.1029/2019GL082485, 2019.

Mouginot, J. and Rignot, E.: Ice motion of the Patagonian icefields of South America: 1984–2014, Geophys. Res. Lett., 42, 1441–1449, https://doi.org/10.1002/2014GL062661, 2015.

Möller, M. and Schneider, C.: Calibration of glacier volume–area relations from surface extent fluctuations and application to future glacier change, J. Glaciol, 56, 33–40, https://doi.org/10.3189/002214310791190866, 2010.

Nelder, J. A. and Mead, R.: A simplex method for function minimization, Comput. J., 7, 308–313, https://doi.org/10.1093/comjnl/7.4.308, 1965.

Réveillet, M., Rabatel, A., Gillet-Chaulet, F., and Soruco, A.: Simulations of changes to Glaciar Zongo, Bolivia (16 S), over the 21st century using a 3-D full-Stokes model and CMIP5 climate projections, Ann. Glaciol., 56, 89–97, https://doi.org/10.3189/2015AoG70A113, 2015.

Rivera, A., Bown, F., Casassa, G., Acuña, C., and Clavero, J.: Glacier shrinkage and negative mass balance in the Chilean Lake District (40 degrees S), Hydrol. Sci. J., 50, https://doi.org/10.1623/hysj.2005.50.6.963, 2005.

Sagredo, E. A., Rupper, S., and Lowell, T. V.: Sensitivities of the equilibrium line altitude to temperature and precipitation changes along the Andes, Quat. Res., 81, 355 – 366, https://doi.org/10.1016/j.yqres.2014.01.008, 2014.

Sakakibara, D. and Sugiyama, S.: Ice-front variations and speed changes of calving glaciers in the Southern Patagonia Icefield from 1984 to 2011, J. Geophys. Res. Earth Surf., 119, 2541–2554, https://doi.org/10.1002/2014JF003148, 2014.

https://doi.org/10.5194/tc-2020-296
Preprint. Discussion started: 11 November 2020

Sauter, T., Arndt, A., and Schneider, C.: COSIPY v1.2 – An open-source coupled snowpack and ice surface energy and mass balance model, Geosci. Model Dev. Discuss., 2020, 1–25, https://doi.org/10.5194/gmd-2020-21, https://gmd.copernicus.org/preprints/gmd-2020-21/, 2020.

Schaefer, M., Machguth, H., Falvey, M., and Casassa, G.: Modeling past and future surface mass balance of the Northern Patagonia Icefield, J. Geophys. Res. Earth Surf., 118, 571–588, https://doi.org/10.1002/jgrf.20038, 2013.

Schaefer, M., Machguth, H., Falvey, M., Casassa, G., and Rignot, E.: Quantifying mass balance processes on the Southern Patagonia Icefield, Cryosphere, 9, 25–35, https://doi.org/10.5194/tc-9-25-2015, 2015.

Schaefer, M., Rodriguez, J. L., Scheiter, M., and Casassa, G.: Climate and surface mass balance of Mocho Glacier, Chilean Lake District, 40 degrees S, J. Glaciol., 63, 218–228, https://doi.org/10.1017/jog.2016.129, 2017.

Scheiter, M.: Ice flow simulations on the Mocho-Choshuenco ice cap, Master Thesis, TU Freiberg, 2019.

Six, D. and Vincent, C.: Sensitivity of mass balance and equilibrium-line altitude to climate change in the French Alps, J. Glaciol., 60, 867–878, https://doi.org/10.3189/2014JoG14J014, 2014.

Taylor, K. E., Stouffer, R. J., and Meehl, G. A.: An overview of CMIP5 and the experiment design, Bull. Am. Meteorol. Soc, 93, 485–498, https://doi.org/10.1175/BAMS-D-11-00094.1, 2012.

Wang, Z., Lin, G., and Ai, S.: How long will an Arctic mountain glacier survive? A case study of Austre Lovénbreen, Svalbard, Polar Res., https://doi.org/10.33265/polar.v38.3519, 2019.

Zemp, M., Huss, M., Thibert, E., Eckert, N., McNabb, R., Huber, J., Barandun, M., Machguth, H., Nussbaumer, S. U., Gärtner-Roer, I., et al.: Global glacier mass changes and their contributions to sea-level rise from 1961 to 2016, Nature, 568, 382–386, https://doi.org/10.1038/s41586-019-1071-0, 2019.